



1 **Reduction in vehicular emissions attributable to the**
2 **Covid-19 lockdown in Shanghai: insights from 5-year**
3 **monitoring-based machine learning**

4 Meng Wang¹, Yusen Duan², Zhuozhi Zhang¹, Qi Yuan¹, Xinwei Li¹, Shuwen Han¹,
5 Juntao Huo², Jia Chen², Yanfen Lin², Qingyan Fu^{2, *}, Tao Wang¹, Junji Cao^{3,4}, Shun-
6 cheng Lee^{1, *}

7 ¹Department of Civil and Environmental Engineering, The Hong Kong Polytechnic University, Hung
8 Hom, Hong Kong SAR, China

9 ²Shanghai Environmental Monitoring Center, Shanghai, China

10 ³State Key Laboratory of Loess and Quaternary Geology, Institute of Earth Environment, Chinese
11 Academy of Sciences, Xi'an 710061, China

12 ⁴Key Laboratory of Middle Atmosphere and Global Environment Observation, Institute of Atmospheric
13 Physics, Chinese Academy of Sciences, Beijing 100029, China

14 *Correspondence to:* shun-cheng.lee@polyu.edu.hk (S.C. Lee) and qingyanf@sheemc.cn (Q.Y. Fu).

15 **Abstract.** Exposure to element carbon (EC) and NO_x is a public health issue that has been gaining
16 increasing interest, with high exposure levels generally observed in traffic environments e.g., roadsides.
17 Shanghai, home to approximately 25 million in the Yangtze River Delta (YRD) region in east China, has
18 one of the most intensive traffic activities in the world. However, our understanding of the trend in
19 vehicular emissions and, in particular, in response to the strict Covid-19 lockdown is limited partly due
20 to a lack of long-term observation dataset and application of advanced mathematical models. In this
21 study, NO_x and EC were continuously monitored at a near highway sampling site in west Shanghai for
22 5 years (2016-2020). The long-term dataset was used to train the machine learning model, rebuilding the
23 NO_x and EC in a business-as-usual (BAU) scenario in 2020. The reduction in NO_x and EC attributable
24 to lockdown was found to be smaller than it appeared because the first week of lockdown overlapped
25 with the lunar new year holiday, whereas, at a later stage of lockdown, the reduction (50-70%)
26 attributable to the lockdown was more significant, confirmed by satellite monitoring of NO₂. In contrast,
27 the impact of the lockdown on vehicular emissions cannot be well represented by simply comparing the
28 concentration before and during the lockdown for conventional campaigns. This study demonstrates the
29 value of continuous air pollutant monitoring at a roadside on a long-term basis. Combined with the
30 advanced mathematical model, air quality changes upon future emission control and/or event-driven
31 scenarios are expected to be better predicted.

32 **1 Introduction**

33 As a response to the Covid-19 outbreak, strict lockdown measures were initiated in major cities across
34 China in 2020, including the megacity of Shanghai in the Yangtze River Delta (YRD) region (He et al.,
35 2020; Wang et al., 2020; Dai et al., 2021; Wu et al., 2021). The lockdown measures generally started in
36 late January and lasted roughly one month, during which normal human activities were constrained
37 substantially (He et al., 2020; Wang et al., 2020). The lockdown measures, such as shutting down cross-
38 city travel and requiring people to stay at home, were strictly implemented to minimize human activities



39 (Zhao et al., 2020; Liu et al., 2020). As a result of these restrictive measures, anthropogenic emissions
40 of air pollutants, in particular, vehicular emissions, have been found to be reduced substantially as
41 evidenced by the evolution of NO₂ which is routinely measured at the ground air quality monitoring site,
42 as well as from the satellite monitoring (He et al., 2020; Li et al., 2021; Wu et al., 2021).

43 The impacts of vehicular emissions of NO₂ on public health are significant both through direct harm
44 on inhalation and as a precursor to secondary pollutants such as ozone and particulate matter (PM) (Lin
45 et al., 2022b; Lyu et al., 2022; Li et al., 2019; Lu et al., 2019). Although NO₂ concentrations are regulated
46 by air quality standards, limitations of NO_x (NO+NO₂) emissions are becoming new emission standards
47 for new vehicles (Grange et al., 2017). In addition to NO_x emission, on-road vehicles were also the major
48 source of primary PM emission, comprising various organic and inorganic species (Lin et al., 2018;
49 Hallquist et al., 2009; Fuzzi et al., 2015; Lin et al., 2020). As a major component of fine PM with a
50 diameter of less than 2.5 μm (PM_{2.5}), elemental carbon (EC) or black carbon is emitted a result of
51 incomplete combustion of fossil fuel (gasoline and diesel) in the internal combustion engine (Lin et al.,
52 2020; Lin et al., 2022a; Jia et al., 2021), with significant health and climate implications (Ramanathan
53 and Carmichael, 2008; Cappa et al., 2012; Rappazzo et al., 2015). With the recent implementation of
54 high emission standards (e.g., China IV and V), gasoline vehicles are generally less polluted, in terms of
55 EC emission when compared to diesel vehicles (Lin et al., 2020; Huang et al., 2022), especially with the
56 recent implementation of high emission standards (e.g., China IV and V). Gasoline-powered vehicles are
57 currently comprising over 90% of the total vehicles in China, with the trend of phasing out of vehicles
58 with old emission standards (i.e., China I–III) (Wang et al., 2019; Wang et al., 2022a). Nevertheless, on-
59 road vehicular emissions are still one of the major sources of NO_x and EC in urban China (Zheng et al.,
60 2018; Zhang et al., 2019). Moreover, the total vehicular emission is also impacted by traffic mix and
61 volume, vehicle ages, and vehicle speed, while meteorological variables e.g., wind speed and wind
62 direction can impact the measured concentrations of air pollutants, making the quantification of vehicular
63 emission challenging in the real-world ambient environment.

64 The strict Covid-19 lockdown measures provided a unique opportunity to study the changes in event-
65 driven vehicular emissions, formulating a scientific basis for designing future air quality mitigation
66 strategies. However, the degree of reduction in vehicular emissions that can be attributable to the Covid-
67 19 outbreak varied greatly in different studies (up to over two-fold differences; (Jia et al., 2020; Wang
68 et al., 2020; Dai et al., 2021; Wu et al., 2021)). For example, by directly comparing the NO_x
69 concentrations before and during the Covid-19 lockdown period, Jia et al. (2020) found a 56-58%
70 reduction in NO_x during the Covid-19 lockdown period in Shanghai. However, the lockdown period
71 overlapped with the Chinese Spring Festival holiday (Wang et al., 2020), during which human activities
72 including traffic were already largely reduced. Moreover, meteorological conditions (e.g., wind speed
73 and direction) may vary, and, therefore, the direct comparison between two different periods does not
74 necessarily reflect the trend in emissions. To decouple the meteorological effects, a meteorological
75 normalization or de-weathering process was first proposed by Grange and Carslaw (2019) using a tree-
76 based machine learning algorithm. Vu et al. (2019) developed the de-weathering process to investigate
77 the seasonal trend of typical air pollutants routinely measured in Beijing and the de-weathered pollutants
78 showed a good agreement with the primary emission from the emission inventory. Using a similar de-



79 weathering process and taking into account the holiday effects. Dai et al. (2021) showed that the
80 reduction (-15.4%) in NO₂ attributable to Covid-19 lockdown was, on average, roughly half of the total
81 reduction (-29.5%) from comparing the measured and counterfactual NO₂ in a business as usual (BAU)
82 scenario during the overlapping period in 31 major Chinese cities. The decline in NO₂ attributable to the
83 lockdowns was also shown to be not as large as expected in 11 cities globally after a de-weathering
84 process (Shi et al., 2021). However, most of these tree-based machine learning studies did not quantify
85 the importance of the input variables, making these the machine learning process non-explainable or like
86 a “black box” (Lin et al., 2022b; Wang et al., 2022a). An explainable machine learning algorithm such as
87 the SHapley Additive exPlanation (SHAP) can quantify the impact of meteorological variables
88 (Lundberg et al., 2020; Qin et al., 2022; Wang et al., 2022a). However, few studies have applied the
89 explainable machine learning algorithm to study the trend in vehicular emissions. Moreover, most
90 previous studies focused on the changes in the measured NO₂ concentrations, which was routinely
91 measured in air quality monitoring site (He et al., 2020; Wang et al., 2020), while few studies reported
92 vehicular EC emissions based on long-term (years) measurement, and therefore, limiting our
93 understanding of vehicular PM_{2.5} emissions under such a policy intervention and more importantly our
94 ability to predict future air quality changes upon similar emission control strategies.

95 Shanghai is an economic center of China, acting as a major transport hub. In 2019, the number of
96 civilian vehicles was over 4 million in Shanghai, approximately 13% higher than that in 2017 (Ministry
97 of Transport, 2020). On average, the daily ridership in Shanghai was over 57 million, with the turnover
98 quantity of motor vehicles of approximately 235 million passenger car unit kilometers (Ministry of
99 Transport, 2020). Because of the intensive traffic activities, exposure to EC has become a public health
100 issue that has been gaining increasing interest, with high individual EC exposure levels generally
101 observed in traffic environments e.g., roadsides (Jia et al., 2021; Zhou et al., 2020). In this study, hourly
102 EC and NO_x were continuously measured for five years (2016-2020) at a near highway sampling site in
103 west Shanghai. A machine-learning model i.e., random forest, was applied to train the model to rebuild
104 the measured EC and NO_x using meteorological and temporal variables as the model input (Grange et
105 al., 2018; Grange and Carslaw, 2019; Grange et al., 2021; Wang et al., 2022a). The SHAP algorithm
106 (Lundberg et al., 2020) was used to quantify the impact of meteorological variables on the measured EC
107 and NO_x. A business-as-usual (BAU) scenario was assumed in 2020 and compared with the measured
108 EC and NO_x, quantifying the reduction attributable to the lockdown measures. Implications of future
109 emission control measures on vehicular emissions are discussed.

110 **2 Method**

111 **2.1 Field sampling**

112 Measurements of the NO_x and EC were conducted continuously from 2016 to 2020 (5 years) at a near
113 highway sampling site at the Dianshan Lake (DSL) supersite (31.09° N, 120.98° E, approximately 15 m
114 above ground), with two highways (G318 and G50) located approximately 1 km west of the sampling
115 site. The sampling site is located in Qingpu District in western Shanghai (Fig. S1), 50 km west of
116 downtown Shanghai. It is at the intersection of Jiangsu, Shanghai, and Zhejiang Provinces. Windrose



117 analysis showed that the sampling site could be affected by the two nearby highways during both 2016-
118 2019 (normal years) and 2020 with Covid-19 lockdown measures implemented (Figure S2).

119 Details of the instrument used to measure EC and NO_x were provided previously (Jia et al., 2020).
120 Briefly, EC was measured on an hourly basis using a Sunset Carbon Analyzer (Model RT-4, Sunset Lab,
121 USA), while hourly NO and NO₂ were monitored using a Thermo Scientific gas analyzers (Thermo 42i,
122 Thermo Fisher Scientific, Massachusetts, USA). Meteorological variables of air temperature (air_temp),
123 wind direction (wd), wind speed (ws), relative humidity (RH), pressure, and rainfall were measured using
124 a Vaisala automatic weather station (WXT520, Vaisala Ltd., Finland).

125 Satellite images of NO₂ were obtained from Sentinel-5P Level-3 Near Real-Time dataset based on the
126 observation of the TROPOspheric Monitoring Instrument (TROPOMI) for 2019 and 2020 (Gorelick et
127 al., 2017). The spatial and temporal distribution of vertical column densities (molecules cm⁻²) of
128 tropospheric NO₂ was used to study the changes in vehicular emissions as a response to strict lockdown
129 measures implemented in 2020.

130 **2.2 Data analysis**

131 **2.2.1 Machine learning set-up and validation**

132 A machine learning algorithm - Random Forest (Grange et al., 2018; Wang et al., 2022a; Wang et al.,
133 2022b) was deployed to understand the impact of Covid-19 lockdown on the exhaust emissions from the
134 near highways in 2020 based on a business as usual (BAU) scenario. NO_x and EC were used as a marker
135 of traffic exhaust emissions as traffic was its main contributor in Shanghai (Jia et al., 2021). In this study,
136 the diurnal patterns of EC and NO_x show typical rush hours peaks during both the normal and Covid-19
137 lockdown periods, consistent with the emission pattern from traffic (Fig. S3).

138 Meteorological (ws, wd, air_temp, RH, rainfall, and pressure) and time (date_unix, day of the year,
139 weekday, hour of the day, and day of the lunar year) variables were used as model inputs to explain the
140 hourly mean EC and NO_x concentrations. The time variable of date_unix is the number of seconds since
141 1 January 1970. Because the day of the lunar new year is different in the Gregorian calendar, it was
142 necessary to include the day of the lunar year to better represent the Chinese New Year holiday, which
143 usually causes a reduction in pollutant concentration during the holiday (Wang et al., 2020; Dai et al.,
144 2021). For each random forest, the number of trees in the forest was set to 300, while a minimal nod size
145 was set to five following e (Grange et al., 2018). The training and testing split percentages were 80% and
146 20% of the dataset, respectively. The random forest model was performed using the latest “rmweather”
147 R package e (Grange et al., 2018).

148 Validation of the developed Random Forest was performed by comparing the time series of the
149 predicted and measured NO_x/EC for both the testing and training dataset (Table S1, discussed in Sect.
150 3.3). The time series of the predicted NO_x/EC showed a good agreement with the measured ones with
151 correlation coefficients in the range of 0.89-0.98 and slopes close to unity, suggesting the developed
152 Random Forest model captured the variation of the target pollutant well.

153 **2.2.2 Quantification of the reduction in pollutants attributable to the Covid-19 lockdown**

154 Based on the developed Random Forest model, the counterfactual NO_x and EC concentrations in a BAU
155 scenario were derived. The BAU scenario assumed everything was the same in 2020 as in the previous
156 years. Because the random forest captured the variation of the target pollutant better than the multi-linear



157 regression model (Table S1), the counterfactual NO_x and EC concentrations reflected the corresponding
158 pollutant in a BAU scenario better. The long-term measurements of NO_x/EC covered multiple years were
159 necessary to train the model as a comparison to short-term sampling. The BAU analysis was performed
160 using a function within the “rmweather” R package (Grange et al., 2018).

161 The counterfactual NO_x/EC concentrations were compared with the measured ones during the holiday
162 (the first week of the lunar year), transition (from day 8 to Lantern Festival, i.e., day 15), and after the
163 transition period, when the lockdown measures were most restrictive. The differences between the
164 counterfactual and measured NO_x/EC are regarded as the portion that can be attributable to the Covid-
165 19 lockdown measures (Grange et al., 2021). Specifically, to get the pollutant concentration in a BAU
166 scenario, a machine learning model was trained by the data over the previous four years to capture the
167 variability of pollutant concentrations using the same input variables as detailed in Sect. 2.3.1. After
168 training, the grown forest was used to predict pollutant concentrations experienced beyond the training
169 period during the Covid-19 lockdown. As a result, the time series of the predicted pollutant beyond the
170 training period is a counterfactual, representing the model estimation of pollutant concentrations during
171 the BAU scenario. The pollutant concentrations in the BAU scenario were subsequently compared with
172 what was observed, with the differences representing the magnitude of the reduction attributable to the
173 of Covid-19 lockdown.

174 2.2.3 Feature importance analysis using the SHAP algorithm

175 In this study, SHAP (<https://github.com/slundberg/shap>) was applied to explain the output of the machine
176 learning model, quantifying the importance of the meteorological variables (Lundberg et al., 2020;
177 Oukawa et al., 2022). SHAP is a game theoretic approach that connects optimal credit allocation with
178 local explanations using the classic Shapley values and their related extensions (Lundberg et al., 2020).
179 SHAP analysis was performed using the python package of SHAP (version 0.41.0) and scikit-learn
180 (version 1.2.0).

181 SHAP produced an interpretable machine-learning model using an additive feature attribution
182 method (Lundberg et al., 2020). SHAP quantified the contribution of the input meteorological variables
183 to a single prediction at a specific time, producing a SHAP value in the same unit as the target pollutant.
184 An overview of which meteorological variables were most important for predicting EC/ NO_x was
185 obtained based on the SHAP values of every feature for every time point. The SHAP overview plot sorted
186 meteorological variables by the sum of SHAP value magnitudes over the entire sampling period. SHAP
187 values were obtained to show the distribution of the impacts each meteorological variables had on the
188 model output.

189 3 Results and Discussion

190 3.1 Trend of observed NO_x during the holiday period and Covid-19 lockdown

191 Figure 1a shows the time series of NO_x for 4 weeks before and after the start of the Chinese lunar new
192 year for 5 years (2016-2020) measurement at the near highway sampling site in west Shanghai (Fig. S1).
193 To understand the impact of the Covid-19 lockdown measurements on traffic emission, we focus on the
194 NO_x time series in 2020 in comparison to the averaged time series of NO_x (grey line) for the previous



195 four years (i.e., the mean of 2016-2019). The beginning of the 2020 lockdown, starting on January 24,
196 overlapped with the start of the Chinese New Year holiday when human activities have already been
197 reduced to a large extent as most migrant workers leave the city for their hometowns. Therefore, the
198 holiday effects need to be taken into account when evaluating the impact of the national lockdown
199 measures on the measured pollutants at the near highway sampling site.

200 For 2016-2019, a large reduction in NO_x was seen during the 7-day holiday period when compared to
201 before the holiday. After the holiday, NO_x levels started to bounce back during the transition period (i.e.,
202 the period before the lantern festival at DOY 15) and finally reached a similar level after the transition
203 period when compared to that before the holiday (Fig. 1a). Specifically, before the holiday, the mean
204 concentration of NO_x was $72.8 \mu\text{g m}^{-3}$, while, during the holiday, NO_x concentration was $22.6 \mu\text{g m}^{-3}$.
205 After the holiday, the NO_x levels increased from $42.6 \mu\text{g m}^{-3}$ during the transition to $60.6 \mu\text{g m}^{-3}$ after
206 the transition period. Assuming a scenario without the holiday effect, as represented by the arrow line in
207 Fig. 1b, a reduction of approximately 65% (or $43 \mu\text{g m}^{-3}$) in the observed NO_x concentration was seen
208 during the holiday when compared to that before the holiday ($72.8 \mu\text{g m}^{-3}$) for 2016-2019.

209 Similar to 2016-2019, the observed NO_x in 2020 was also largely reduced (60%) during the holiday
210 period when compared to before the holiday (Fig. 1b). Specifically, the NO_x before the holiday was 79.5
211 $\mu\text{g m}^{-3}$, while it was $29.0 \mu\text{g m}^{-3}$ during the holiday. Because the Covid-19 lockdown started on the same
212 day as the holiday, the reduction in NO_x observed at the sampling site attributable to the lockdown
213 measures was smaller than it appeared. In other words, simply comparing the air pollutant concentration
214 during the first 7-day of lockdown to that before the lockdown would overestimate the impact of Covid-
215 19 on the measured air pollutant when holiday effects were strong.

216 However, NO_x remained at low levels during the transition and after the transition period in 2020, i.e.,
217 the last two weeks during the lockdown, instead of rapidly rising as observed in 2016-2019 (Fig. 1). The
218 mean concentration during the transition period was $32.6 \mu\text{g m}^{-3}$ and was $34.8 \mu\text{g m}^{-3}$ for the last two
219 weeks during the lockdown in 2020, which was 25% and 50% lower, respectively, when compared to
220 the same period for 2016-2019. Because it usually takes some time for the control measure to take effect,
221 focusing on the first 7-day of the lockdown may not represent the true impact of the Covid-19 lockdown
222 on air quality. Instead, as the lockdown measures took effect, a large reduction in NO_x can be seen at the
223 late stages of the lockdown when NO_x was supposed to be increasing. Therefore, we focused on the
224 comparison of NO_x during the last two weeks of the lockdown (labeled as “lockdown” in Fig. 1 and
225 afterward if not specified otherwise) to study the impact of lockdown measures on traffic emission at
226 this sampling site.

227 3.2 Observed EC reduction attributable to the lockdown control policies

228 The measured EC at the near highway sampling site showed a diurnal pattern with a clear morning
229 rush hour peak, consistent with that for NO_x (Fig. S3), suggesting EC was mainly affected by the nearby
230 traffic. The measured EC also showed a dependence on wind speed and wind direction, with a higher
231 concentration associated with low wind speed from the southwest direction, i.e., from the highway (Fig.
232 S4). The conclusion of EC being mainly from traffic is consistent with previous source apportionment
233 studies in Shanghai (Chang et al., 2018; Jia et al., 2021).



234 Figure 2 shows the time series of EC before and during the 2020 lockdown as well as the average time
235 series of EC (grey line) for the previous four years (i.e., the mean of 2016-2019). Similar to NO_x, the
236 2016-2019 EC level during the holiday was reduced due to the reduced traffic (Fig. 2). Specifically, the
237 mean EC concentration was 1.08 μg m⁻³ during the holiday, roughly 40% lower compared to that (1.74
238 μg m⁻³) before the holiday. During the transition period for 2016-2019, EC increased to 1.03 μg m⁻³.
239 Afterward, EC increased to 1.53 μg m⁻³, very close to the levels before the holiday.

240 For the 2020 CNY holiday or the first week of the Covid-19 lockdown, EC was also reduced to a
241 similar level (0.88 μg m⁻³) as 2016-2019 (1.08 μg m⁻³; Fig. 2). Similar to NO_x, the EC reduction
242 attributable to the lockdown measures was not as large as it appeared for the period overlapping with the
243 holiday. However, EC remained at a low level during (0.92 μg m⁻³) and after the transition (0.78 μg m⁻³)
244 period. This is because the month-long lockdown measures kept the traffic at a low level for a prolonged
245 time. This is consistent with the pattern observed for NO_x, further confirming the measured EC and NO_x
246 at this near highway sampling site were mainly from traffic emissions. The mean EC concentration
247 during the transition period or roughly the second week of lockdown in 2020 was 10 % lower than the
248 same period for 2016-2019, while the mean EC concentration during the last two weeks of lockdown
249 was 50% lower than the same period for 2016-2019. The low level of EC during and after the transition
250 period was due to the lockdown measures, reducing the traffic volume and, therefore, reducing the
251 corresponding traffic-related EC emission.

252 3.3 Rebuilding the measured NO_x and EC using a machine learning algorithm

253 The measured mass concentrations of atmospheric NO_x and EC were affected by the meteorological
254 variables including wind speed and wind direction (Fig. S4). This is particularly true for multiple years
255 of measurement when the meteorological variables varied over these years. Therefore, the concentration
256 measured at different years was not directly comparable when meteorological variables were varying in
257 addition to emission strength across years. Moreover, the relationship between the measured NO_x/EC
258 and meteorological conditions was not linear. This is demonstrated by the poor correlation coefficient
259 (R=0.45-0.48) between the rebuilt NO_x/EC and the meteorological parameters using the multilinear
260 regression model (Table S1). Therefore, the multilinear regression model failed to rebuild the measured
261 NO_x/EC satisfactorily. In this study, the non-linear relationship between NO_x/EC and the meteorological
262 variables was captured by a machine learning algorithm - random forest (See the method section).

263 Figure 3a shows the scatter plot between the time series of the rebuilt and measured NO_x for the
264 training and testing dataset. The predicted NO_x was well correlated with the measured NO_x with a
265 correlation coefficient (R) of 0.89-0.98, suggesting over 80 % of the data (R²>0.8) can be explained by
266 the machine learning model. This value is higher than that from the multilinear regression model (Table
267 S1). Therefore, the machine learning model demonstrated a better performance than the multilinear
268 regression model in capturing the relationship between the NO_x and meteorological variables.

269 Figure 3b shows the scatter plot between the time series of the predicted and measured EC for the
270 training and testing dataset. Similar to NO_x, the rebuilt EC was well correlated with the measured EC
271 with a correlation coefficient (R) of 0.9-0.98, suggesting over 80 % of the EC can be explained by the
272 machine learning model. However, for both NO_x and EC, the slope for the linear fit was in the range of



273 0.67-0.85, suggesting the predicted values were, on average, 13-33% lower than the measured values.
274 By examining the data, the lower than unity slope was mainly caused by the data points with high
275 concentrations. These data points can be regarded as outliers that were not captured properly by the
276 machine learning model since these data points deviated largely from the averaged values.

277 In this study, meteorological variables were used as input variables to train the machine learning model
278 to rebuild the observed NO_x and EC. However, different meteorological variables had different roles in
279 affecting the measured NO_x and EC, showing different levels of importance. To evaluate the importance
280 of different meteorological variables, SHAP model was applied (See method section). Figure 4 shows
281 the SHAP values (in $\mu\text{g m}^{-3}$) obtained during the rebuilding of NO_x and EC. The meteorological variable
282 with a high SHAP value was associated with high importance, whereas a SHAP value closer to zero
283 means the meteorological variable was less important. For NO_x , ws is the most important meteorological
284 variable (Fig. 4), with low ws contributing up to over $100 \mu\text{g m}^{-3}$ and high ws contributing negatively to
285 NO_x (down to $-40 \mu\text{g m}^{-3}$). Air temperature, RH, wd, and pressure had SHAP values in the range of -40
286 $\mu\text{g m}^{-3}$ to $70 \mu\text{g m}^{-3}$, while rainfall was least important with SHAP values of $<10 \mu\text{g m}^{-3}$ (Fig. 4). Similarly,
287 ws was also the important variable for EC, with low ws contributing positively to the EC (SHAP value
288 of up to over $2 \mu\text{g m}^{-3}$, Fig. 4). Wd, pressure, air temperature, and RH had similar SHAP values ($<1.5 \mu\text{g}$
289 m^{-3}). Although rainfall was less important, high rainfall was associated with low SHAP values, consistent
290 with the wet deposition of aerosol.

291 **3.4 Trend of meteorologically normalized NO_x and EC: a business-as-usual scenario**

292 To evaluate the impact of the lockdown in 2020 on the NO_x/EC emission at this near highway sampling
293 site, a business-as-usual (BAU) scenario was assumed. The BAU scenario in 2020 assumed that
294 everything was similar to what would happen previously, i.e., without the lockdown measures. For the
295 BAU scenario in 2020, NO_x and EC would drop during the holiday, but increase their concentration
296 levels during the transition and reach a similar level to that before the holiday (Fig. 5), similar to that
297 observed in 2016-2019 (Fig. 1 and 2). Through the comparison of the 2020 BAU to the measured
298 NO_x/EC in 2020, the reduction in NO_x/EC attributable to Covid-19 can be quantitatively evaluated.

299 The NO_x and EC concentrations during the holiday, transition, and lockdown period were normalized
300 to that before the holiday (Fig. 5). For BAU in 2020, the NO_x during the holiday was reduced to 53% of
301 the level for that before the holiday. In comparison, the measured NO_x during the holiday was 36% of
302 the level before the holiday. Therefore, the difference (17%) between BAU-2020 and 2020 was
303 attributable to the Covid-19 control measures. In other words, the measured NO_x was roughly 30%
304 (17%/53%) lower than what would be without the control measures. During the transition period, the
305 NO_x level for BAU-2020 returned to $\sim 75\%$ of the level before the holiday. In comparison, the measured
306 NO_x was only 40% of that before the holiday. Therefore, the measured NO_x was approximately 45%
307 lower than the BAU-2020. After the transition period, NO_x returned to a similar level to that before the
308 holiday for BAU-2020. However, the measured NO_x was only 40% of that before the holiday. As a result,
309 the NO_x reduction attributable to the Covid-19 lockdown measures was the most significant after the
310 transition period, which was approximately 60% of the BAU-2020. Therefore, the month-long lockdown



311 measures kept the NO_x at a low level consistently, demonstrating the effectiveness of the lockdown in
312 reducing traffic emissions as the lockdown measures continued.

313 Similar to NO_x , EC also showed the largest reduction during lockdown when compared to the BAU
314 2020 (Fig. 5b). Specifically, EC was roughly 60% lower during the lockdown in 2020 than the BAU
315 scenario in 2020, while the reduction in EC was 40% and 30% lower during the transition and holiday
316 period, respectively. As a result, both NO_x and EC showed a similar level of reduction which were
317 attributable to the lockdown measures.

318 **3.5 Reduction in traffic emission during the Covid-19 lockdown confirmed by satellite monitoring**

319 Figure 6 shows the TROPOMI images of NO_2 in the YRD region over the same period, i.e., before the
320 holiday and after the transition, for the years 2019 and 2020. By comparing the vertical column densities
321 of NO_2 monitored over the same period in 2019 and 2020, the evolution of satellite-monitoring of NO_2
322 showed a consistent trend with that observed from the ground monitoring at the near highway sampling
323 site (Fig. 1-3). In particular, a great reduction (50-70%) in NO_2 during the lockdown period in 2020 was
324 seen when compared to that over the same period in 2019, whereas after the transition period in 2020,
325 NO_2 was expected to return to a similar level as that before the holiday i.e., the BAU scenario discussed
326 in Sect 3.4. Therefore, the reduction (50-70%) in NO_2 in 2020 was attributable to the lockdown measures
327 based on the knowledge gained from the surface monitoring site.

328 Specifically, the vertical column concentration of NO_2 at the DSL was highly elevated before the
329 holiday in 2019 with mean vertical column concentrations of over 18×10^{15} molecules cm^{-2} . After the
330 transition period in 2019, NO_2 returned to a slightly lower value ($16-18 \times 10^{15}$ molecules cm^{-2}) compared
331 to that before the holiday. This is consistent with BAU scenario assumed in 2020 (Fig. 5). In 2020, NO_2
332 before the holiday was similar to the level over the same period in 2019 ($18-20 \times 10^{15}$). However, during
333 the lockdown period, the NO_2 was $8-10 \times 10^{15}$, 50-70% lower than in the same period in 2019. Such a
334 reduction was attributable to the lockdown measures.

335 **4 Discussion**

336 Through the comparison of EC and NO_x before and during the lockdown in 2020, as well as the same
337 period in the previous years (2016-2019), we showed that the reduction in vehicular emissions that can
338 be attributed to the lockdown measures was complicated and cannot be achieved by simply comparing
339 the concentration difference between before and during the lockdown. This is because vehicular
340 emissions have their own trend during the Chinese holiday when vehicular emission was largely reduced
341 (Dai et al., 2021). Here, we show that, due to the overlapping of the first week of lockdown with the
342 holiday, the reduction in vehicular emission attributable to the lockdown was smaller than it appeared.
343 This trend can be only revealed from multiple years of continuous measurement and would be easily
344 missed by a conventional field campaign that only lasted months. This is consistent with the previous
345 studies (Shi et al., 2021; Dai et al., 2021; He et al., 2020). However, in addition to the holiday effects,
346 we showed that the reduction in vehicular emission was nearly entirely attributable to the lockdown at a
347 later stage of lockdown, whereas the holiday and transition period only lasted for 2 weeks.



348 The lockdown in Shanghai 2020 provided a unique opportunity to study the impact of strict emission
349 control on local and regional air quality. Many studies have shown the impact of lockdown on traffic
350 emission, but with different degrees of impact partly because the duration of the lockdown was month-
351 long and partly overlapped with the holiday as shown in this study (Jia et al., 2020; Dai et al., 2021; Shi
352 et al., 2021; Wang et al., 2020). However, most previous studies focused on gas pollutant i.e., NO₂
353 probably because NO₂ was a regular gas pollutant that is routinely measured at the air quality monitoring
354 sites across the major Chinese cities (He et al., 2020), while few reported the particulate EC emission
355 from traffic partly due to the scarcity of the dataset. EC is light absorbing and is regarded as a warming
356 agent second to CO₂ (Cappa et al., 2012; Jacobson, 2001; Liu et al., 2015). In addition, EC is one of the
357 major particulate pollutants that can cause adverse health effects (Daellenbach et al., 2020; Rappazzo et
358 al., 2015). To the best of our knowledge, this is the first study to illustrate the impact of lockdown on
359 vehicular EC emissions at a near highway sampling site based on 5-years of continuous measurement.
360 Such a dataset is rare in the literature since lockdown measures restrict the movement of instrument
361 operators. Only with good maintenance of the instrument at the sampling site can we keep the sampling
362 going on during the strict lockdown.

363 To decouple the effects of the meteorological variables on the measured NO_x and EC, a machine
364 learning model was trained and tested based on the 5-year dataset. The machine learning model emerges
365 as a powerful model in air quality studies especially the development of SHAP (Lundberg et al., 2020)
366 making the machine learning model explainable rather than a black box as in most previous air quality
367 studies (Grange and Carslaw, 2019; Grange et al., 2017; Shi et al., 2021; Vu et al., 2019). The explainable
368 machine learning model of SHAP showed meteorological variables especially ws and wd were key
369 parameters that affect the measured levels with concentrations of up to 100 µg m⁻³ for NO_x. Due to
370 important the role of meteorological variables, their impact needs to be removed when evaluating the
371 true impact of the lockdown on vehicular emissions. Here, instead of simply comparing the concentration
372 before and during the lockdown, a BAU scenario was assumed in 2020. This relies on the rebuilding
373 power of the mathematical model. However, to train the machine learning model, a large body of datasets
374 is required as input. As more datasets are to be collected and used as model input, the performance of
375 machine learning is expected to improve further. Moreover, with more variables, e.g., vehicular types,
376 weight, and road conditions, being monitored and used as input for the model, a better prediction power
377 of the machine learning is anticipated. Correspondingly, the air quality improvement upon future
378 emission control scenarios can be better predicted.

379 **5 Conclusion**

380 In this study, the time series of vehicular emissions of NO_x and EC before and during the 2020 lockdown
381 as well as the averaged time series of NO_x over the same period for the previous four years (i.e., the mean
382 of 2016-2019) were compared and used to train the machine learning model, rebuilding the NO_x and EC
383 in a BAU scenario in 2020. Meteorological variables especially wind speed and direction were found to
384 be the key parameters that affect the measured levels with concentrations of up to 100 µg m⁻³ for NO_x
385 using the explainable machine learning model of SHAP. Due to important the role of meteorological
386 variables, their impact needs to be removed when evaluating the true impact of the lockdown on vehicular



387 emissions. In contrast, by simply comparing the concentration before and during the lockdown, the
388 effects of the lockdown on air pollutant emission can be misrepresented. The results show that vehicular
389 emissions had their own trend during the Chinese holiday during which vehicular emission was largely
390 reduced. Because the first week of lockdown overlapped with the holiday, the reduction in vehicular
391 emissions attributable to the lockdown was smaller than it appeared. This is in line with previous studies
392 that took into account the holiday effects using a machine learning based de-weathering process.
393 However, different from previous studies, a large reduction (50-70%) in vehicular emissions of NO_x and
394 EC was attributed to the lockdown at a later stage. This value is larger than previous studies because both
395 the holiday effects and meteorological impacts were removed during this period. This large reduction in
396 vehicular emissions at a later stage was confirmed by satellite monitoring of NO₂. Therefore, strict
397 lockdown reduced both vehicular gaseous and particulate emission significantly when holiday and
398 meteorological effects were not affecting the trend analysis. This study demonstrates the importance of
399 continuous monitoring at this Shanghai supersite. When coupled with an advanced mathematical
400 algorithm, insights into the impact of human activities on air pollution can be gained based on long-term
401 monitoring. Air quality improvement in future emission control scenarios is expected to be better
402 predicted.

403 **Associate content**

404 Supporting Information
405 Supplementary figures (Fig. S1-S4).

406 **Credit authorship contribution statement**

407 MW, ZZ, XL and SH designed the study. YD, JH, JC, YL and QF conducted field campaign. MW, YD,
408 ZZ and QY conducted data analysis. MW prepared the manuscript with contributions from all co-authors.
409 QF, TW, JC and SL provided input for revision before submission. QF and SL provided project guidance.

410 **Declaration of competing interest**

411 The authors declare that they have no conflicting interests.

412 **Acknowledgements**

413 This work was supported by the Start-up Fund for RAPs under the Strategic Hiring Scheme (P0043854),
414 Green Tech Fund (GTF202110151), Environment and Conservation Fund-Environmental Research,
415 Technology Demonstration and Conference Projects (ECF 63/2019), the RGC Theme-based Research
416 Scheme (T24-504/17-N), the RGC Theme-based Research Scheme (T31-603/21-N), Key Research and
417 Development Projects of Shanghai Science and Technology Commission (20dz1204000), State Ecology
418 and Environment Scientific Observation and Research Station for the Yangtze River Delta at Dianshan
419 Lake (SEED).



References

- Cappa, C. D., Onasch, T. B., Massoli, P., Worsnop, D. R., Bates, T. S., Cross, E. S., Davidovits, P., Hakala, J., Hayden, K. L., Jobson, B. T., Kolesar, K. R., Lack, D. A., Lerner, B. M., Li, S.-M., Mellon, D., Nuaaman, I., Olfert, J. S., Petäjä, T., Quinn, P. K., Song, C., Subramanian, R., Williams, E. J., and Zaveri, R. A.: Radiative Absorption Enhancements Due to the Mixing State of Atmospheric Black Carbon, *Science*, 337, 1078-1081, <https://doi.org/10.1126/science.1223447>, 2012.
- Chang, Y., Huang, K., Xie, M., Deng, C., Zou, Z., Liu, S., and Zhang, Y.: First long-term and near real-time measurement of trace elements in China's urban atmosphere: temporal variability, source apportionment and precipitation effect, *Atmospheric Chemistry and Physics*, 18, 11793-11812, <https://doi.org/10.5194/acp-18-11793-2018>, 2018.
- Daellenbach, K. R., Uzu, G., Jiang, J., Cassagnes, L.-E., Leni, Z., Vlachou, A., Stefenelli, G., Canonaco, F., Weber, S., Segers, A., Kuenen, J. J. P., Schaap, M., Favez, O., Albinet, A., Aksoyoglu, S., Dommen, J., Baltensperger, U., Geiser, M., El Haddad, I., Jaffrezo, J.-L., and Prévôt, A. S. H.: Sources of particulate-matter air pollution and its oxidative potential in Europe, *Nature*, 587, 414-419, <https://doi.org/10.1038/s41586-020-2902-8>, 2020.
- Dai, Q., Hou, L., Liu, B., Zhang, Y., Song, C., Shi, Z., Hopke, P. K., and Feng, Y.: Spring Festival and COVID-19 Lockdown: Disentangling PM Sources in Major Chinese Cities, *Geophysical Research Letters*, 48, e2021GL093403, <https://doi.org/10.1029/2021GL093403>, 2021.
- Fuzzi, S., Baltensperger, U., Carslaw, K., Decesari, S., Denier Van Der Gon, H., Facchini, M., Fowler, D., Koren, I., Langford, B., and Lohmann, U.: Particulate matter, air quality and climate: lessons learned and future needs, *Atmospheric Chemistry and Physics*, 15, 8217-8299, <https://doi.org/10.5194/acp-15-8217-2015>, 2015.
- Gorelick, N., Hancher, M., Dixon, M., Ilyushchenko, S., Thau, D., and Moore, R.: Google Earth Engine: Planetary-scale geospatial analysis for everyone, *Remote Sensing of Environment*, 202, 18-27, <https://doi.org/10.1016/j.rse.2017.06.031>, 2017.
- Grange, S. K. and Carslaw, D. C.: Using meteorological normalisation to detect interventions in air quality time series, *Science of The Total Environment*, 653, 578-588, <https://doi.org/10.1016/j.scitotenv.2018.10.344>, 2019.
- Grange, S. K., Lewis, A. C., Moller, S. J., and Carslaw, D. C.: Lower vehicular primary emissions of NO₂ in Europe than assumed in policy projections, *Nature Geoscience*, 10, 914-918, <https://doi.org/10.1038/s41561-017-0009-0>, 2017.
- Grange, S. K., Carslaw, D. C., Lewis, A. C., Boleti, E., and Hueglin, C.: Random forest meteorological normalisation models for Swiss PM₁₀ trend analysis, *Atmospheric Chemistry and Physics*, 18, 6223-6239, <https://doi.org/10.5194/acp-18-6223-2018>, 2018.
- Grange, S. K., Lee, J. D., Drysdale, W. S., Lewis, A. C., Hueglin, C., Emmenegger, L., and Carslaw, D. C.: COVID-19 lockdowns highlight a risk of increasing ozone pollution in European urban areas, *Atmospheric Chemistry and Physics*, 21, 4169-4185, <https://doi.org/10.5194/acp-21-4169-2021>, 2021.
- Hallquist, M., Wenger, J. C., Baltensperger, U., Rudich, Y., Simpson, D., Claeys, M., Dommen, J., Donahue, N. M., George, C., Goldstein, A. H., Hamilton, J. F., Herrmann, H., Hoffmann, T., Iinuma, Y.,



- Jang, M., Jenkin, M. E., Jimenez, J. L., Kiendler-Scharr, A., Maenhaut, W., McFiggans, G., Mentel, T. F., Monod, A., Prévôt, A. S. H., Seinfeld, J. H., Surratt, J. D., Szmigielski, R., and Wildt, J.: The formation, properties and impact of secondary organic aerosol: current and emerging issues, *Atmospheric Chemistry and Physics*, 9, 5155-5236, <https://doi.org/10.5194/acp-9-5155-2009>, 2009.
- He, G., Pan, Y., and Tanaka, T.: The short-term impacts of COVID-19 lockdown on urban air pollution in China, *Nature Sustainability*, 3, 1005-1011, <https://doi.org/10.1038/s41893-020-0581-y>, 2020.
- Huang, H., Zhang, J., Hu, H., Kong, S., Qi, S., and Liu, X.: On-road emissions of fine particles and associated chemical components from motor vehicles in Wuhan, China, *Environmental Research*, 210, 112900, <https://doi.org/10.1016/j.envres.2022.112900>, 2022.
- Jacobson, M. Z.: Strong radiative heating due to the mixing state of black carbon in atmospheric aerosols, *Nature*, 409, 695-697, [10.1038/35055518](https://doi.org/10.1038/35055518), 2001.
- Jia, H., Huo, J., Fu, Q., Duan, Y., Lin, Y., Jin, X., Hu, X., and Cheng, J.: Insights into chemical composition, abatement mechanisms and regional transport of atmospheric pollutants in the Yangtze River Delta region, China during the COVID-19 outbreak control period, *Environmental Pollution*, 267, 115612, <https://doi.org/10.1016/j.envpol.2020.115612>, 2020.
- Jia, H., Pan, J., Huo, J., Fu, Q., Duan, Y., Lin, Y., Hu, X., and Cheng, J.: Atmospheric black carbon in urban and traffic areas in Shanghai: Temporal variations, source characteristics, and population exposure, *Environmental Pollution*, 289, 117868, <https://doi.org/10.1016/j.envpol.2021.117868>, 2021.
- Li, K., Jacob, D. J., Liao, H., Zhu, J., Shah, V., Shen, L., Bates, K. H., Zhang, Q., and Zhai, S.: A two-pollutant strategy for improving ozone and particulate air quality in China, *Nature Geoscience*, 12, 906-910, <https://doi.org/10.1038/s41561-019-0464-x>, 2019.
- Li, K., Jacob, D. J., Liao, H., Qiu, Y., Shen, L., Zhai, S., Bates, K. H., Sulprizio, M. P., Song, S., Lu, X., Zhang, Q., Zheng, B., Zhang, Y., Zhang, J., Lee, H. C., and Kuk, S. K.: Ozone pollution in the North China Plain spreading into the late-winter haze season, *Proceedings of the National Academy of Sciences*, 118, <https://doi.org/10.1073/pnas.2015797118>, [10.1073/pnas.2015797118](https://doi.org/10.1073/pnas.2015797118), 2021.
- Lin, C., Huang, R.-J., Duan, J., Zhong, H., Xu, W., Wu, Y., and Zhang, R.: Large contribution from worship activities to the atmospheric soot particles in northwest China, *Environmental Pollution*, 299, 118907, <https://doi.org/10.1016/j.envpol.2022.118907>, 2022a.
- Lin, C., Huang, R. J., Zhong, H., Duan, J., Wang, Z., Huang, W., and Xu, W.: Elucidating ozone and PM_{2.5} pollution in Fenwei Plain reveals the co-benefits of controlling precursor gas emissions in winter haze, *EGUsphere*, 2022, 1-15, <https://doi.org/10.5194/egusphere-2022-1440>, 2022b.
- Lin, C., Ceburnis, D., Xu, W., Heffernan, E., Hellebust, S., Gallagher, J., Huang, R. J., O'Dowd, C., and Ovadnevaite, J.: The impact of traffic on air quality in Ireland: insights from the simultaneous kerbside and suburban monitoring of submicron aerosols, *Atmospheric Chemistry and Physics*, 20, 10513-10529, <https://doi.org/10.5194/acp-20-10513-2020>, 2020.
- Lin, C., Huang, R.-J., Ceburnis, D., Buckley, P., Preissler, J., Wenger, J., Rinaldi, M., Facchini, M. C., O'Dowd, C., and Ovadnevaite, J.: Extreme air pollution from residential solid fuel burning, *Nature Sustainability*, 1, 512-517, <https://doi.org/10.1038/s41893-018-0125-x>, 2018.
- Liu, T., Wang, X., Hu, J., Wang, Q., An, J., Gong, K., Sun, J., Li, L., Qin, M., Li, J., Tian, J., Huang, Y., Liao, H., Zhou, M., Hu, Q., Yan, R., Wang, H., and Huang, C.: Driving Forces of Changes in Air Quality



during the COVID-19 Lockdown Period in the Yangtze River Delta Region, China, *Environmental Science & Technology Letters*, 7, 779-786, <https://doi.org/10.1021/acs.estlett.0c00511>, 2020.

Liu, Z., Guan, D., Wei, W., Davis, S. J., Ciais, P., Bai, J., Peng, S., Zhang, Q., Hubacek, K., Marland, G., Andres, R. J., Crawford-Brown, D., Lin, J., Zhao, H., Hong, C., Boden, T. A., Feng, K., Peters, G. P., Xi, F., Liu, J., Li, Y., Zhao, Y., Zeng, N., and He, K.: Reduced carbon emission estimates from fossil fuel combustion and cement production in China, *Nature*, 524, 335-338, <https://doi.org/10.1038/nature14677>, 2015.

Lu, K., Fuchs, H., Hofzumahaus, A., Tan, Z., Wang, H., Zhang, L., Schmitt, S. H., Rohrer, F., Bohn, B., Broch, S., Dong, H., Gkatzelis, G. I., Hohaus, T., Holland, F., Li, X., Liu, Y., Liu, Y., Ma, X., Novelli, A., Schlag, P., Shao, M., Wu, Y., Wu, Z., Zeng, L., Hu, M., Kiendler-Scharr, A., Wahner, A., and Zhang, Y.: Fast Photochemistry in Wintertime Haze: Consequences for Pollution Mitigation Strategies, *Environmental Science & Technology*, 53, 10676-10684, <https://doi.org/10.1021/acs.est.9b02422>, 2019.

Lundberg, S. M., Erion, G., Chen, H., DeGrave, A., Prutkin, J. M., Nair, B., Katz, R., Himmelfarb, J., Bansal, N., and Lee, S.-I.: From local explanations to global understanding with explainable AI for trees, *Nature Machine Intelligence*, 2, 56-67, <https://doi.org/10.1038/s42256-019-0138-9>, 2020.

Lyu, X., Guo, H., Zou, Q., Li, K., Xiong, E., Zhou, B., Guo, P., Jiang, F., and Tian, X.: Evidence for Reducing Volatile Organic Compounds to Improve Air Quality from Concurrent Observations and In Situ Simulations at 10 Stations in Eastern China, *Environmental Science & Technology*, <https://doi.org/10.1021/acs.est.2c04340>, 2022.

<https://www.ceicdata.com/en/china/no-of-motor-vehicle-private-owned/cn-no-of-motor-vehicle-private-owned-shanghai> (Last Access: 5 August 2022), last.

Oukawa, G. Y., Krecl, P., and Targino, A. C.: Fine-scale modeling of the urban heat island: A comparison of multiple linear regression and random forest approaches, *Science of The Total Environment*, 815, 152836, <https://doi.org/10.1016/j.scitotenv.2021.152836>, 2022.

Qin, X., Zhou, S., Li, H., Wang, G., Wang, X., Fu, Q., Duan, Y., Lin, Y., Huo, J., Huang, K., and Deng, C.: Simulation of Spatiotemporal Trends of Gaseous Elemental Mercury in the Yangtze River Delta of Eastern China by an Artificial Neural Network, *Environmental Science & Technology Letters*, 9, 205-211, <https://doi.org/10.1021/acs.estlett.1c01025>, 2022.

Ramanathan, V. and Carmichael, G.: Global and regional climate changes due to black carbon, *Nature Geoscience*, 1, 221, <https://doi.org/10.1038/ngeo156>, 2008.

Rappazzo, K. M., Daniels, J. L., Messer, L. C., Poole, C., and Lobdell, D. T.: Exposure to Elemental Carbon, Organic Carbon, Nitrate, and Sulfate Fractions of Fine Particulate Matter and Risk of Preterm Birth in New Jersey, Ohio, and Pennsylvania (2000-2005), *Environmental Health Perspectives*, 123, 1059-1065, <https://doi.org/10.1289/ehp.1408953>, 2015.

Shi, Z., Song, C., Liu, B., Lu, G., Xu, J., Vu, T. V., Elliott, R. J. R., Li, W., Bloss, W. J., and Harrison, R. M.: Abrupt but smaller than expected changes in surface air quality attributable to COVID-19 lockdowns, *Science Advances*, 7, eabd6696, <https://doi.org/10.1126/sciadv.abd6696>, 2021.

Vu, T. V., Shi, Z., Cheng, J., Zhang, Q., He, K., Wang, S., and Harrison, R. M.: Assessing the impact of clean air action on air quality trends in Beijing using a machine learning technique, *Atmospheric Chemistry and Physics*, 19, 11303-11314, <https://doi.org/10.5194/acp-19-11303-2019>, 2019.



Wang, J., Wu, Q., Liu, J., Yang, H., Yin, M., Chen, S., Guo, P., Ren, J., Luo, X., Linghu, W., and Huang, Q.: Vehicle emission and atmospheric pollution in China: problems, progress, and prospects, *PeerJ*, 7, e6932-e6932, <https://doi.org/10.7717/peerj.6932>, 2019.

Wang, M., Duan, Y., Zhang, Z., Huo, J., Huang, Y., Fu, Q., Wang, T., Cao, J., and Lee, S.-c.: Increased contribution to PM_{2.5} from traffic-influenced road dust in Shanghai over recent years and predictable future, *Environmental Pollution*, 313, 120119, <https://doi.org/10.1016/j.envpol.2022.120119>, 2022a.

Wang, M., Zhang, Z., Yuan, Q., Li, X., Han, S., Lam, Y., Cui, L., Huang, Y., Cao, J., and Lee, S.-c.: Slower than expected reduction in annual PM_{2.5} in Xi'an revealed by machine learning-based meteorological normalization, *Science of The Total Environment*, 841, 156740, <https://doi.org/10.1016/j.scitotenv.2022.156740>, 2022b.

Wang, Y., Wen, Y., Wang, Y., Zhang, S., Zhang, K. M., Zheng, H., Xing, J., Wu, Y., and Hao, J.: Four-Month Changes in Air Quality during and after the COVID-19 Lockdown in Six Megacities in China, *Environmental Science & Technology Letters*, 7, 802-808, <https://doi.org/10.1021/acs.estlett.0c00605>, 2020.

Wu, C.-L., Wang, H.-W., Cai, W.-J., He, H.-d., Ni, A.-N., and Peng, Z.-R.: Impact of the COVID-19 lockdown on roadside traffic-related air pollution in Shanghai, China, *Building and environment*, 194, 107718-107718, <https://doi.org/10.1016/j.buildenv.2021.107718>, 2021.

Zhang, Q., Zheng, Y., Tong, D., Shao, M., Wang, S., Zhang, Y., Xu, X., Wang, J., He, H., Liu, W., Ding, Y., Lei, Y., Li, J., Wang, Z., Zhang, X., Wang, Y., Cheng, J., Liu, Y., Shi, Q., Yan, L., Geng, G., Hong, C., Li, M., Liu, F., Zheng, B., Cao, J., Ding, A., Gao, J., Fu, Q., Huo, J., Liu, B., Liu, Z., Yang, F., He, K., and Hao, J.: Drivers of improved PM_{2.5} air quality in China from 2013 to 2017, *Proc. Natl. Acad. Sci.*, 116, 24463-24469, <https://doi.org/10.1073/pnas.1907956116>, 2019.

Zhao, Y., Zhang, K., Xu, X., Shen, H., Zhu, X., Zhang, Y., Hu, Y., and Shen, G.: Substantial changes in nitrate oxide and ozone after excluding meteorological impacts during the COVID-19 outbreak in mainland China, *Environmental Science & Technology Letters*, 402-408, <https://doi.org/10.1021/acs.estlett.0c00304>, 2020.

Zheng, B., Tong, D., Li, M., Liu, F., Hong, C., Geng, G., Li, H., Li, X., Peng, L., Qi, J., Yan, L., Zhang, Y., Zhao, H., Zheng, Y., He, K., and Zhang, Q.: Trends in China's anthropogenic emissions since 2010 as the consequence of clean air actions, *Atmospheric Chemistry and Physics*, 18, 14095-14111, <https://doi.org/10.5194/acp-18-14095-2018>, 2018.

Zhou, H., Lin, J., Shen, Y., Deng, F., Gao, Y., Liu, Y., Dong, H., Zhang, Y., Sun, Q., Fang, J., Tang, S., Wang, Y., Du, Y., Cui, L., Ruan, S., Kong, F., Liu, Z., and Li, T.: Personal black carbon exposure and its determinants among elderly adults in urban China, *Environment International*, 138, 105607, <https://doi.org/10.1016/j.envint.2020.105607>, 2020.

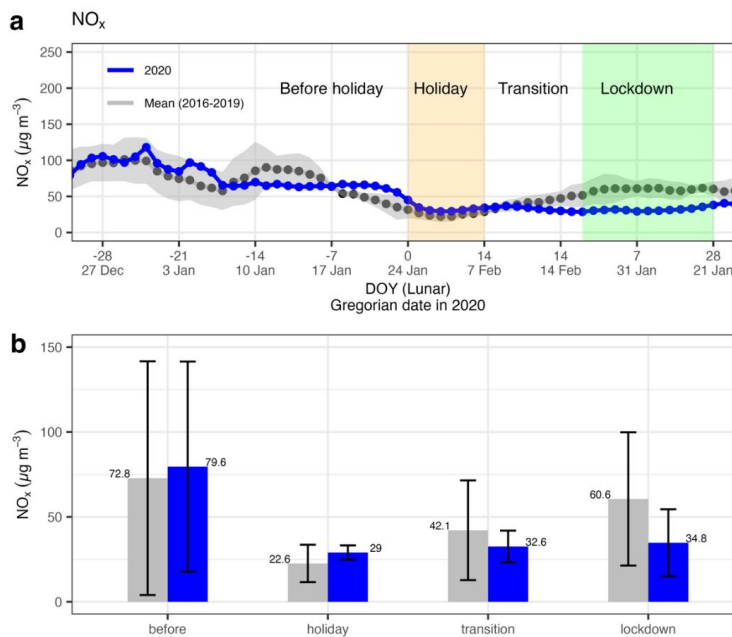


Figure 1. (a) Time series (day of the year; DOY) of the measured NO_x for 4 weeks before and after the start of the Chinese Lunar year for the mean of 2016-2019 and 2020; and (b) Mean NO_x concentrations for different periods, i.e., before the holiday, holiday, transition and lockdown. The time series in (a) was a 7-day rolling average. The error bar in (b) stands for one standard deviation. Note that the lunar DOY for 2016-2019 was on different Gregorian date, but were grouped together based on lunar DOY in (a).

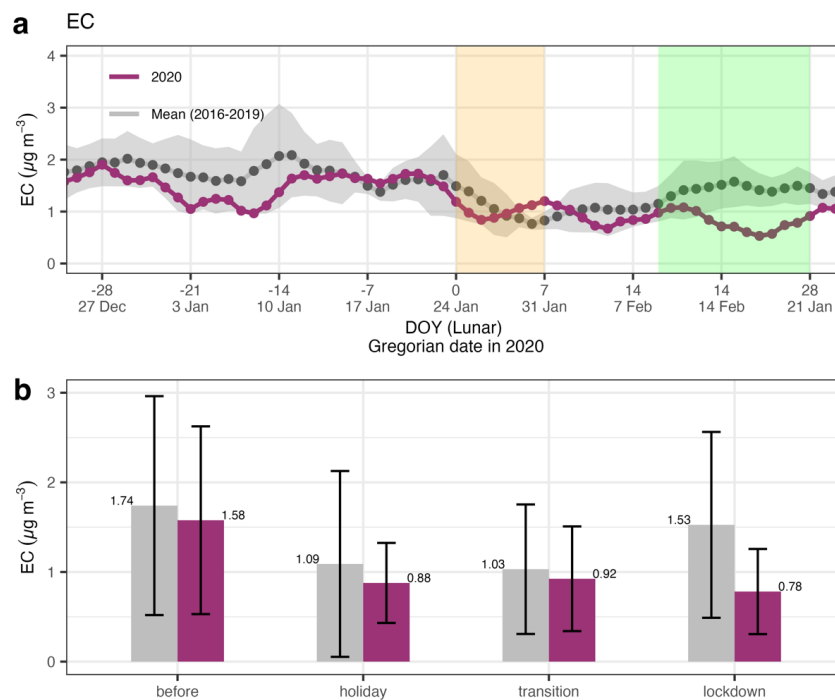


Figure 2. (a) Time series (day of the year; DOY) of the measured EC for 4 weeks before and after the start of the Chinese Lunar year for the mean of 2016-2019 and 2020; and (b) Mean EC concentrations for different periods, i.e., before the holiday, holiday, transition and lockdown. The time series in (a) was a 7-day rolling average. The error bar in (b) stands for one standard deviation.

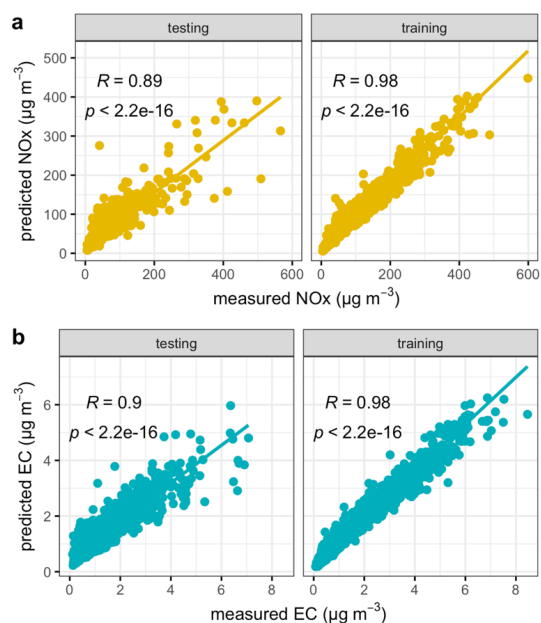


Figure 3. Scatter plot between the predicted and measured (a) NO_x and (b) EC for the testing and training dataset. Also shown is the linear regression between the predicted and measured values, with the correlation coefficient (*R*) and *p*-value in the top left.

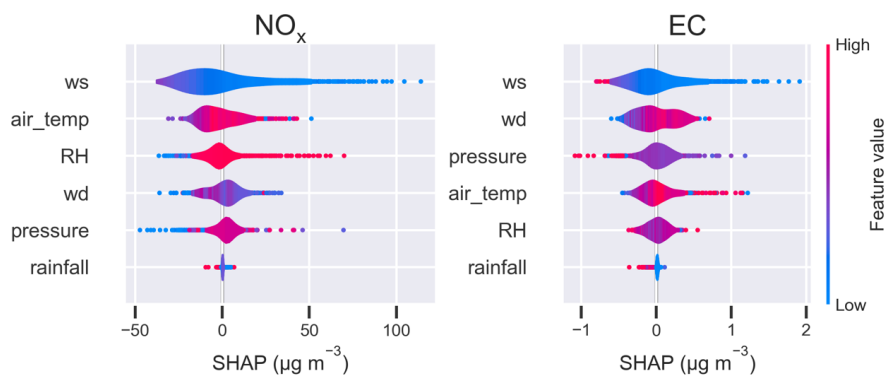


Figure 4. SHAP values (in $\mu\text{g m}^{-3}$) for the meteorological variables i.e., features when building the random forest model for NO_x and EC.

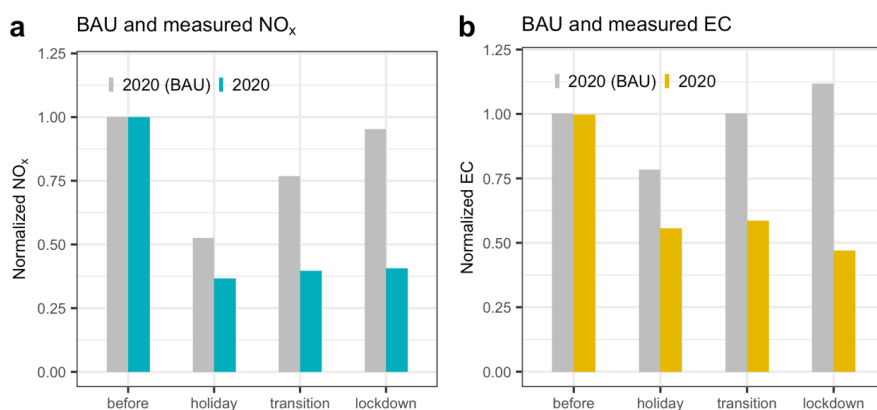


Figure 5. Comparison of NO_x (a) and EC (b) evolution between the business-as-usual (BAU) scenario and the measured one in 2020. All concentrations were normalized to the level before the holiday.

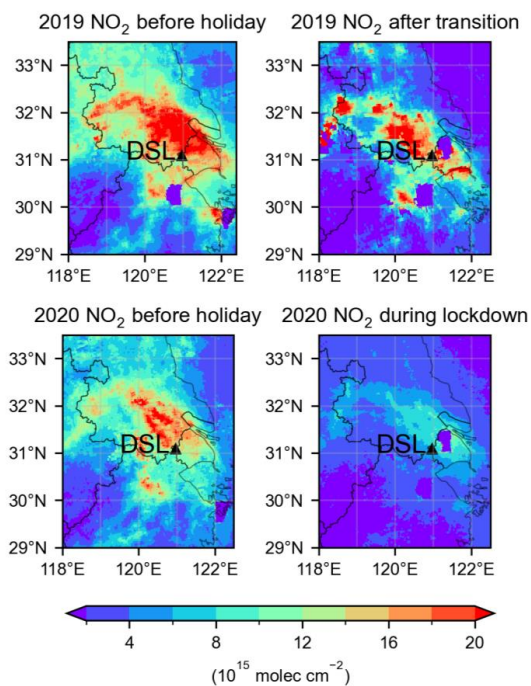


Figure 6. The spatial distribution of TROPOMI NO₂ over the same period in 2019 and 2020 near the DSL sampling site in west Shanghai in the YRD region.